communications biology

A Nature Portfolio journal

Article

https://doi.org/10.1038/s42003-025-07970-8

Differential response of tissue engineered skeletal muscle from rheumatoid arthritis patients and healthy controls

Check for updates

Catherine E. Oliver[1], Jonathan L. Carter[1], James S. Hong[1], Mingzhi Xu[1], William E. Kraus[2], Kim M. Huffman[2] & George A. Truskey[1]

Rheumatoid arthritis (RA) is a chronic inflammatory disease affecting articular joints and skeletal muscle. To assess the role of cytokines upon muscle strength in RA, we developed an in vitro tissue-engineered human skeletal muscle model (myobundle). Myobundles were generated using primary skeletal muscle cells from the *vastus lateralis* muscle of RA patients and age-matched healthy controls. RA myobundles were more sensitive to 5 ng/mL IFN-γ, exhibiting reduced contractile force and altered contraction kinetics. Addition of IL-6 with or without IFN-γ led to a small but significant increase in striated fibers. Gene sets involved in the response to hypoxia, MTOR1 signaling, and the unfolded protein response were enriched in IFN-γ-treated RA myobundles, but not IFN-γ-treated controls. Tofacitinib increased contractile force and myosin heavy chain levels and restored PIM1 protein levels in RA myobundles treated with IFN-γ. Thus, in RA muscle, low levels of IFN-γ selectively increase gene pathways that reduce contractile force.

Rheumatoid arthritis (RA) is a chronic inflammatory disease causing pain, increased mortality, and profound disability[1]. RA affects articular joints and multiple organs, including skeletal muscle[2,3]. Loss of muscle mass and strength paralleled by increased fat mass affects up to two-thirds of all RA patients and is associated with reduced physical function and increased disability, especially in women[4–12]. Compared to healthy subjects, RA patients have increased rates of whole-body protein breakdown[13]. Pro-inflammatory cytokines reduce myocyte protein synthesis and increase protein degradation and may promote muscle loss and disability in patients with RA[14].

IL-6 is involved in the development of joint and systemic inflammation of RA[15]. In RA patients, IL-6 is elevated in synovial fluid, skeletal muscle[14], and serum, relative to healthy conditions (1–5 pg/mL)[16], and these levels correlate with RA disease activity[15]. Acute IL-6 exposure stimulates hypertrophic muscle growth and myogenesis by regulating muscle stem cell proliferation[17]. Exposure to elevated levels of IL-6 causes atrophy and muscle wasting via the Janus kinase/signal transducer and activator of transcription (JAK/STAT) pathway[17]. In patients with RA, muscle concentrations of inflammatory markers are positively associated with disease activity (IL-1β, IL-8), disability (IL-1β, IL-6), pain (IL-1β, TNF-α), and physical inactivity (IL-1β, IL-6)[14].

Likewise, IFN-γ is elevated in autoinflammatory and autoimmune diseases[18]. Interferons activate the JAK/STAT pathway and induce expression of canonical interferon-stimulated genes associated with antigen presentation, autoimmunity, and inflammation[18]. Interferons program cell responses to environmental cues, influencing the priming and training of innate immune memory among other effects[18]. Furthermore, synovial IFN-γ expression is sensitive to JAK inhibitors, suggesting inhibition of IFN-γ signaling[18].

Disease-modifying antirheumatic drugs (DMARDs), primarily methotrexate (MTX), are administered as first-line medication for patients newly diagnosed with RA. MTX inhibits nuclear factor-κB (NF-κB) and other pro-inflammatory properties of key cell types involved in RA pathogenesis (T cells, macrophages, endothelial cells, and fibroblasts-like synoviocytes)[19–21]. If RA is not well controlled by DMARD treatment, then biological therapy is initiated. JAK inhibitors (e.g., tofacitinib) are the most recent drug class of disease-modifying RA medication[22]. JAK inhibitors are small molecules that modulate cytokines critical to the progression of RA and are the first oral treatment to compare favorably to existing DMARDs[22]. JAK inhibitors have comparable efficacy to TNF-α inhibitors for American College of Rheumatology (ACR) response rates and disease activity (DAS28) scores[22].

Tissue-engineered skeletal muscle can serve as a platform for disease modeling and drug testing. Our engineered human skeletal muscle constructs (myobundles)[23–25] generate quantitative contractile forces in response to electrical stimulation. The 3D myobundles are amenable to measurement of contractile force, kinetics and fatigue as well as calcium dynamics[23]. Exercise conditions can be simulated[26]. Experiments of duration 2–3 weeks can be

[1]Department of Biomedical Engineering, Duke University, Durham, NC, USA. [2]Department of Medicine, Duke University School of Medicine, Durham, NC, USA. e-mail: george.truskey@duke.edu

performed with the myobundles measuring response to various treatments, whereas in 2D, the myotubes often detach after a few days. Detachment of myofibers in 2D culture limits such experiments. Furthermore, the simple fabrication method of myobundles allows for easy reproducibility in other scientific laboratories and the small scale of this system enables higher throughput at a lower cost compared to animal models.

The goal of this work was to develop an in vitro myobundle model of RA and test potential therapeutics that can reduce muscle damage and loss in RA. We generated myobundles made with cells from the *vastus lateralis* muscle of RA patients and aged-matched healthy controls. Compared to myobundles generated from controls, RA myobundles were more sensitive to treatment with the pro-inflammatory cytokine IFN-γ leading to reduced contractile force. RNA sequencing (RNA-seq) and gene set enrichment analysis (GSEA) were performed to identify gene sets associated with altered gene expression. Gene sets enriched in IFN-γ-treated RA myobundles, but not IFN-γ-treated controls, involved genes upregulated in response to hypoxia and the unfolded protein response. PIM1 and MT-1 were identified as potential therapeutic targets for treating RA-associated muscle dysfunction. PIM1 protein was elevated in RA myobundles after incubation with IFN-γ. After exposure of RA myobundles to IFN-γ, treatment with tofacitinib increased contractile force and myosin heavy chain levels and restored PIM1 protein levels in RA myobundles with IFN-γ-induced dysfunction.

Results

Donor characteristics

Skeletal muscle biopsies of the *vastus lateralis* were obtained from 6 RA patients, aged 61–79 (BMI 21.2–31.9) and 5 age-matched healthy controls, aged 62–76 (BMI 20.6–32.9). All 6 RA patients were female (Supplementary Table 1). Of the healthy controls, 3 were female and 2 were male. RA donors, for which the DAS28 score was known, had disease scores indicating moderate disease activity ($3.2 < DAS28 \leq 5.1$). Other demographic characteristics and laboratory values of the RA patients and controls are shown in Supplementary Table 1.

Contractile forces and kinetics of RA and control myobundles treated with IFN-γ with and without IL-6

To identify cytokines that differentially affected RA and healthy control myobundle contractile force, preliminary experiments were first conducted with RA myobundles from one donor which were differentiated for 7 days and exposed to combinations of IL-1β, IL-6, TNF-α, and IFN-γ for 3 days (Supplementary Fig. 1A, B). At the dose used (5 ng/mL), only IFN-γ caused a reduction in specific twitch or tetanus force.

Next, we compared the response of 5 RA donors and 3 healthy control donors that were differentiated for 7 days and then treated for 3 days with either no cytokines, 5 ng/mL IFN-γ, 5 ng/mL IL-1β + 5 ng/mL IL-6 + 5 ng/mL TNF-α, or 5 ng/mL IL-1β + 5 ng/mL IL-6 + 5 ng/mL TNF-α + 5 ng/mL IFN-γ, followed immediately by measurement of contractile force and determination of specific contractile force (force per cross-sectional area) (Supplementary Fig. 2). None of the treatments affected contractile force in healthy myobundles. Treatment with 5 ng/mL IFN-γ significantly reduced all contractile forces in RA but addition of IL-1β, TNF-α, and IL-6 did not further reduce contractile force.

Based on this we examined the RA and control myobundle response after 7 days treatment to IFN-γ and IL-6. While we did not observe an effect of IL-6 after 3 day treatment, we continued to use it because of its role in RA. RA and age-matched control myobundles were differentiated for 7 days to allow myobundles to mature and then treated chronically with either 5 ng/mL IFN-γ, 5 ng/mL IL-6, or 5 ng/mL IFN-γ + 5 ng/mL IL-6 for 7 days, from day 7 to day 14 of differentiation, followed by testing for contractile force, histology, protein expression, and RNA sequencing.

A two-way ANOVA indicated that the interaction between RA disease and cytokine treatment significantly affected specific twitch force ($p = 0.0484$), but RA and cytokine treatment alone was not significant (Fig. 1A). A post hoc Tukey's test did not detect any pairwise differences. A two-way ANOVA indicated that cytokine treatment ($p < 0.0001$) and the interaction between cytokine treatment and RA disease ($p = 0.0087$) significantly affected specific tetanus force. A post-hoc Tukey test indicated that without any treatment, RA myobundles had higher specific tetanus forces than control myobundles (Fig. 1B), as we noted previously[24]. In RA myobundles, treatment with IFN-γ as well as IFN-γ plus IL-6 reduced specific tetanus force, whereas for control myobundles the addition of IL-6 led to greater tetanus forces relative to control myobundles treated with IFN-γ alone. Based on these results, IL-6 appeared to have little effect on RA myobundle force production for the conditions studied.

From a two-way ANOVA, RA disease significantly affected twitch time to maximum force ($p = 0.0107$) but no significant difference was observed with a post hoc Tukey test (Fig. 1C). For twitch half-relaxation time, RA myobundles were significantly different than control myobundles for all treatment conditions (Fig. 1D).

The trends in contractile force observed for the pooled data in response to cytokine treatment were also observed with the individual donors. For control donors, there was no decrease in specific twitch force with either IFN-γ or IL-6 alone or together (Supplementary Fig. 3), although IL-6 did lead to an increased twitch force with C109 (Supplementary Fig. 3). For specific tetanus force. only one control donor (C111) showed a decrease in contractile force with IFN-γ treatment. Two RA donors exhibited a decrease in twitch force following treatment with IFN-γ treatment, RA104 and RA107 (Supplementary Fig. 4). All RA donors showed a decrease in specific tetanus force after IFN-γ treatment, and 3 donors showed decreased specific tetanus force with IFN-γ and IL-6 treatment relative to IL-6 treatment (Supplementary Fig. 4).

In control myobundles, IFN-γ with and without IL-6 or IL-6 alone reduced fatigue relative to no treatment (Supplementary Fig. 5). In RA myobundles, fatigue was unaffected by IFN-γ or IL-6 treatment.

Myofiber analysis of RA and control myobundles treated with IFN-γ with and without IL-6

Longitudinal sections of cytokine-treated myobundles immunostained for sarcomeric α-actinin (SAA) and nuclei were examined between RA donors and control donors (Fig. 2A, B) and appeared similar under all conditions. There was no effect of RA disease or cytokine treatment on SAA+ area (Supplementary Fig. 6A), myofiber orientation (Supplementary Fig. 6C), and fiber length (Supplementary Fig. 6D). A two-way ANOVA indicated that RA disease significantly affected fraction nuclei in SAA+ fibers ($p = 0.0196$) (Supplementary Fig. 6B) and percent striated fibers ($p < 0.0001$) (Supplementary Fig. 6E). Surprisingly, in RA myobundles, IFN-γ treatment led to a higher fraction of nuclei in SAA+ striated fibers relative to healthy myobundles (Supplementary Fig. 6B). The percent of striated fibers was larger in RA myobundles than control myobundles for the cases of no treatment, IL-6, and IFN-γ with IL-6 (Supplementary Fig. 6E).

Muscle protein analysis of RA and control myobundles treated with IFN-γ with and without IL-6

Western blot for myosin heavy chain (MYH), soluble IL-6 receptor (IL-6R), and myosin light chain (MYL) were compared to a β-actin control for 5 RA donors and 3 controls (Fig. 3A) and the results quantified (Fig. 3B–D). Since the IL-6R signal may have been affected by the β-actin band, particularly for RA myobundles, we ran separate gels in which we stained for IL-6R and β-actin on different lanes of the gel (Supplementary Fig. 7). As a result, background was reduced and the effect on IL-6R of treatment of RA myobundles with IFN-γ with or without IL-6 is noticeable.

A two-way ANOVA indicated that in RA myobundles there was no effect of disease type or cytokine treatment (IFN-γ with or without IL-6) on MYH protein levels. There was an interaction effect between the disease and cytokine treatment conditions ($p = 0.0455$) as noted by the differences between RA myobundle treated with IFN-γ and control bundles that were untreated or treated with IL-6 (Fig. 3B). Additionally, RA ($p < 0.0001$) and cytokine treatment ($p < 0.01$) significantly affected IL-6R levels (Fig. 3C). Furthermore, a significant interaction effect was observed between disease and treatment conditions ($p = 0.0004$) (Fig. 3C). RA disease and cytokine did not affect MYL levels (Fig. 3D).

Fig. 1 | Contractile forces and twitch force kinetics of RA and control myobundles treated with IFN-γ with and without IL-6 for 7 days. A Specific twitch force, **B** specific tetanus force, **C** twitch time to reach maximum force, and **D** twitch half-relaxation time of RA and control myobundles. $N = 5$ RA donors (RA104 (●), RA106 (■), RA107 (▼), RA108 (□), RA109 (▲)); $N = 3$ control donors (C107 (●), C109 (■), C111 (▲)); $n = 3$–5 myobundles per donor. Data are represented as mean ± S.D. and analyzed with a two-way ANOVA followed by Tukey HSD post-hoc test. P values are shown for cases in which $p < 0.05$ for within treatment or for RA/control myobundles between treatments.

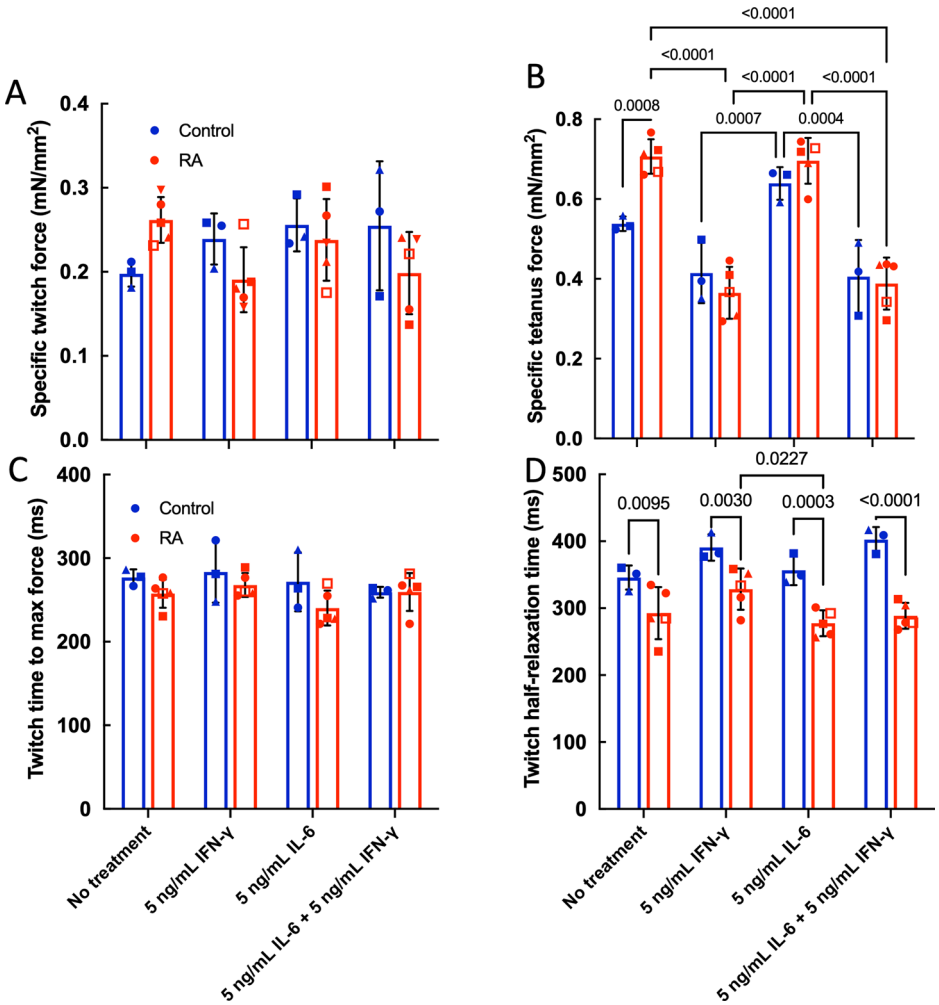

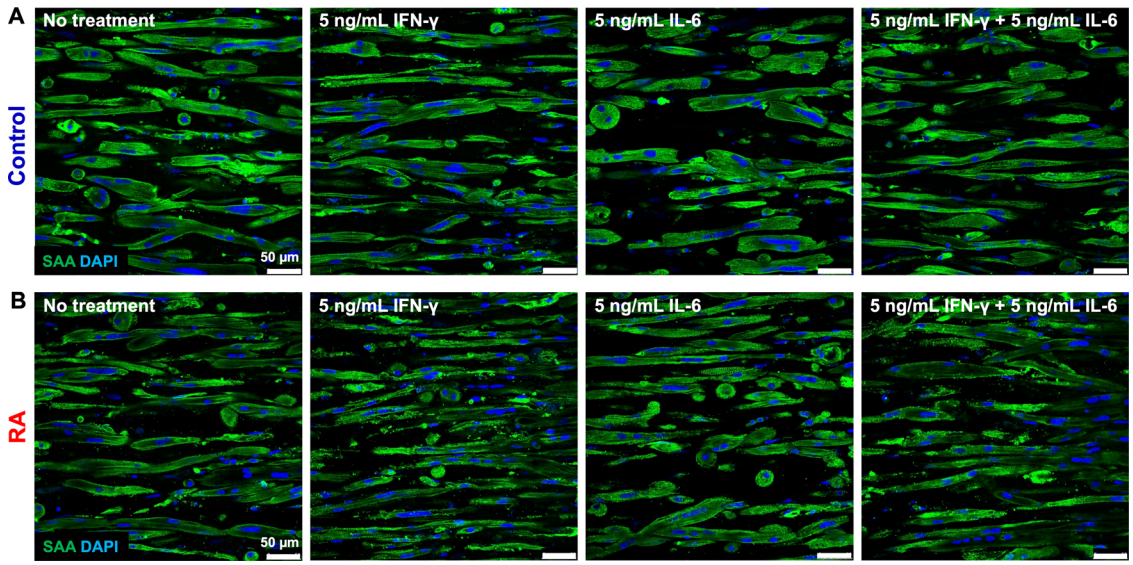

Fig. 2 | Representative longitudinal sections at 40x magnification of RA and control myobundles treated with IFN-γ with and without IL-6 for 7 days. **A** Control and (**B**) RA myobundles were fixed and immunostained for SAA and nuclei at day 14 of differentiation after 7 days of treatment with IFN-γ with and without IL-6. Results are shown for RA donor RA106 and control donor C111. Scale bar = 50 μm.

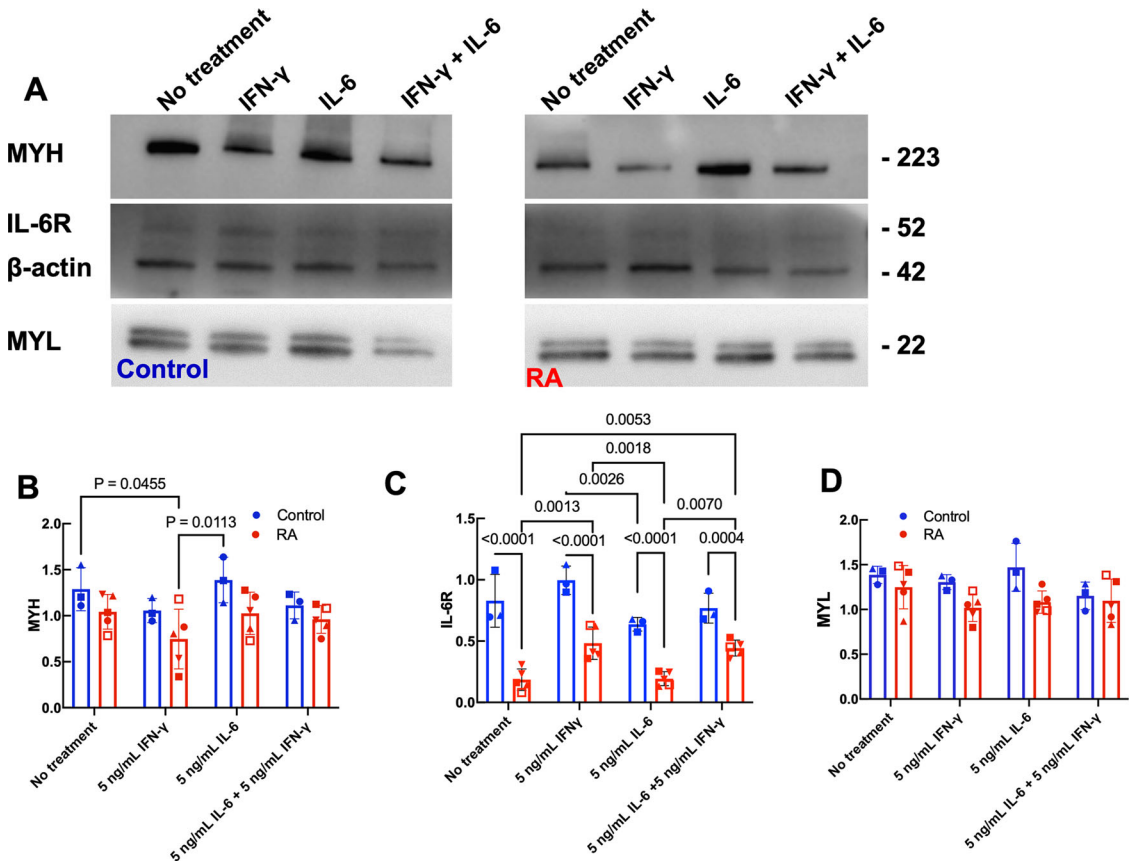

Fig. 3 | Western blot of contractile proteins and IL-6 soluble receptors in RA and control myobundles for 7 days. A Western blot of MYH, IL-6R, and MYL in one RA donor (RA106) and one control (C109) on day 14 of differentiation after 7 days of treatment with IFN-γ with and without IL-6. Quantified expression of (**B**) MYH, (**C**) IL-6R, and (**D**) MYL normalized to β-actin for RA and controls. $N = 5$ RA donors (RA104 (●), RA106 (■), RA107(▲), RA108 (□), and RA109(▼)), 3 control donors (C109 (●), C111(■), C113(▲)). 4 myobundles were pooled together per condition per donor to obtain protein sample. Data are represented as mean ± S.D. and analyzed with two-way ANOVA, followed by Tukey HSD post-hoc.

IL-6R levels were lower in RA myobundles compared to controls for IFN-γ treatment (Fig. 3C). Treatment of control myobundles with IFN-γ with or without IL-6 elevated IL-6R, whereas only the combination of IFN-γ and IL-6 affected IL-6R levels in RA myobundles. This finding is consistent with force results where IL-6-treated RA myobundles produced greater specific tetanus force compared to IFN-γ-treated RA myobundles (Fig. 1B). These results suggest an inverse association between RA force production and RA contractile protein levels in response to IL-6, which is supported by linear regression of specific tetanus force v. IL-6R levels (Supplementary Fig. 8). No correlation between specific tetanus force and protein levels was observed for MYH or MYL. These results suggest additional factors beyond MYL and MYH contractile protein levels affected the response of RA myobundles to IFN-γ.

RNA-sequencing analysis of RA and control myobundles treated with IFN-γ with and without IL-6

Principal components analysis and heatmaps. To determine genes and pathways most affected in RA versus control myobundles treated with IFN-γ with and without IL-6 for 7 days, RNA-sequencing was performed for 3 RA donors and 3 age-matched controls after cytokine treatment. A principal components analysis (PCA) plot of the gene expression results indicated that IFN-γ produced the largest effect on PC1 for RA and control myobundles. Samples that were either untreated or treated with IL-6 appeared to cluster together, whereas samples treated with IFN-γ with or without IL-6 clustered together (Fig. 4A). IL-6 had minimal effect in PC1 or PC2 (Fig. 4A). These trends agreed with our force results for RA myobundles in which IFN-γ reduced specific tetanus force whereas IL-6 had no effect on force alone or when combined with IFN-γ (Fig. 1A, B). PC2 within the PCA plot showed variability among donors, in which control donors were more variable than RA donors with or without IFN-γ treatment (Fig. 4A). However, it should be noted that the 8% variance associated with PC2 was significantly less than the 60% variance associated with PC1 (Fig. 4A).

A heatmap and dendrogram were produced for the top 250 differentially expressed genes for cytokine-treated control myobundles and RA myobundles relative to untreated conditions (Fig. 4B). Each column represents the results for a separate donor. The dendrogram indicates that the primary clustering of the donor samples is between those with and without IFN-γ treatment. Within each of those conditions, the control and RA samples form separate clusters. For each donor, IL-6 treatment is adjacent to the corresponding untreated or IFN-γ treatment case, which is consistent with the force results in which treatment with IL-6 did not affect contractile force.

Differential changes in gene expression after IFNγ treatment. Since treatment with IFN-γ alone induced the largest effect on gene expression for RA myobundles and controls (Fig. 4), we focused our attention on that treatment group. Gene expression was significantly affected in 573 genes for RA and 545 different genes for controls for FDR ≤ 0.05 and $|\log2FC| > 2$ (Fig. 5A). Gene expression was significantly affected in RA and controls for 421 of the same genes (Fig. 5A). Volcano plots displaying gene expression results for treatment with IFN-γ in control and RA myobundles are shown in Fig. 5B, C, respectively. The top 10 most significantly upregulated genes that also pertain to one or more gene sets that were enriched in RA and controls, respectively, are labeled in the volcano plots. The trends are very similar to those observed for the conditions that included IL-6 treatments (Supplementary Fig. 9).

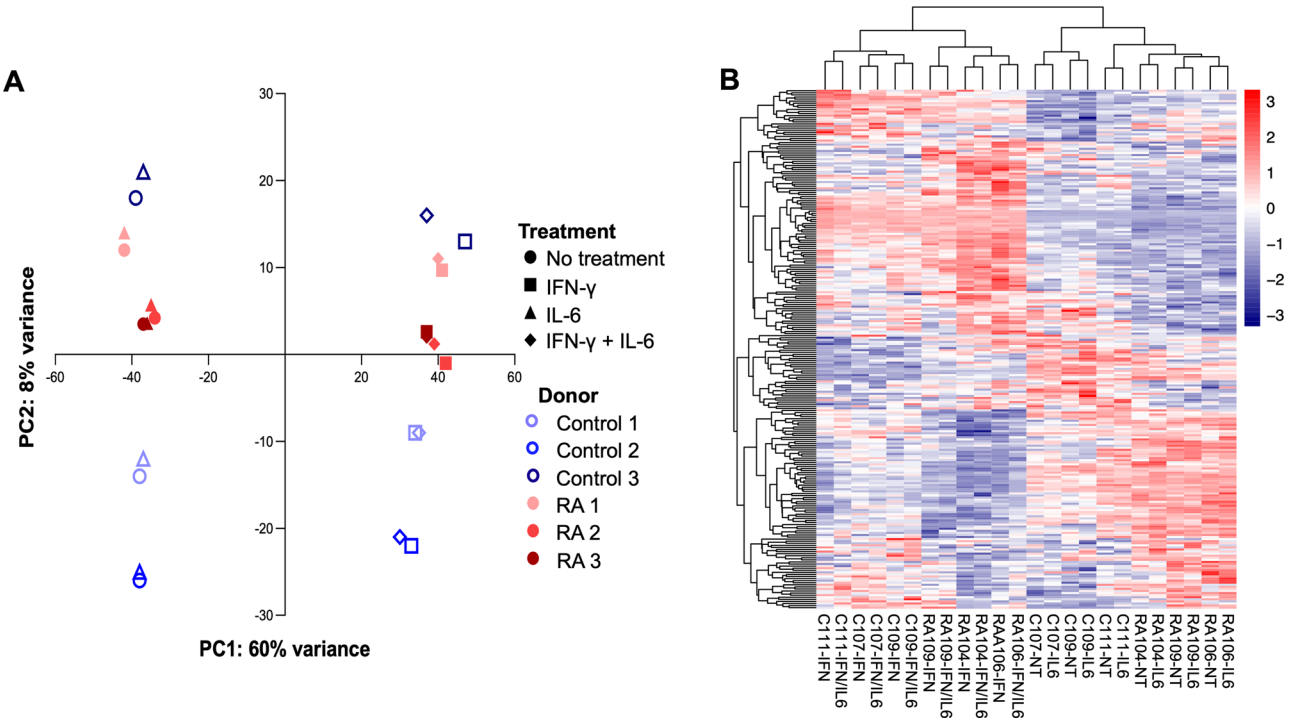

Fig. 4 | Gene expression analysis of RA and control myobundles treated with and without IFN-γ. A Principal components analysis (PCA) and (**B**) heatmap with dendrograms of gene expression of RA and control myobundles treated with IFN-γ with and without IL-6 for 7 days relative to corresponding untreated conditions (NT). RA and control myobundles were flash frozen on day 14 of differentiation prior to RNA isolation. $N = 3$ RA donors (RA104, RA106, RA109 corresponding to RA 1, RA 2 and RA 3, respectively), 3 control donors (C107, C109, C111, corresponding to Control 1, Control 2 and Control 3, respectively); $n = 4$ myobundle RNA samples per donor, except $n = 3$ myobundles for C111 IFN-γ condition. Myobundles were pooled together per condition per donor.

A

	Control +IFN-γ/ Untreated Control Myobundles	RA+IFN-γ/ Untreated RA Myobundles	Overlap
Downregulated	55	57	61
Upregulated	69	95	360

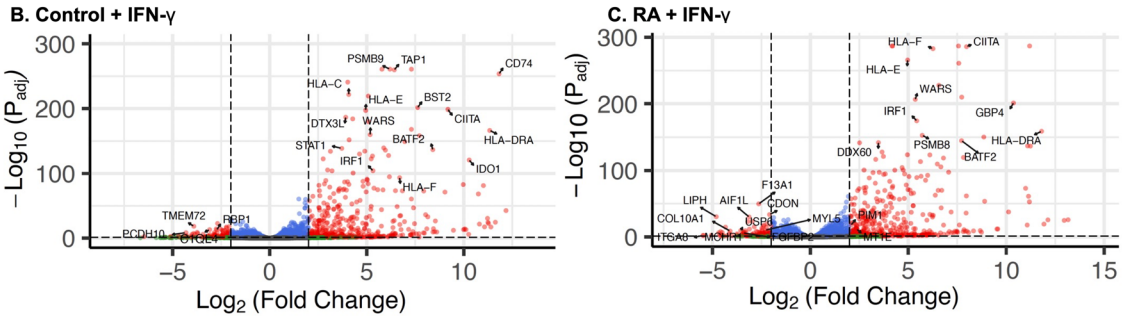

Fig. 5 | Differential gene expression of IFN-γ-treated RA and control myobundles. RA and control myobundles were treated with IFN-γ for 7 days from day 7 to day 14 of differentiation. **A** Number of significant genes between IFN-γ-treated RA myobundles and IFN-γ-treated controls, (**B**) volcano plot showing up- and down-regulated genes for IFN-γ-treated controls relative to untreated controls, and (**C**) volcano plot showing up- and down-regulated genes for IFN-γ-treated RA myobundles relative to untreated RA myobundles. Gene expression results for IFN-γ-treated RA and control myobundles were normalized to respective untreated controls. $N = 3$ RA donors, 3 control donors; $n = 4$ myobundle RNA samples per donor, except $n = 3$ for RA111 IFN-γ condition. The donors are the same as those listed in Fig. 4. Myobundles were pooled together per condition per donor. $|\log2FC| \geq 2$, $p_{adj} < 0.05$.

Although IFN-γ treatment did not reduce MYH and MYL contractile protein levels in RA myobundles compared to controls, the antibodies were not specific for individual isoforms. To assess any effect on the expression of any effect on contractile protein isoforms, we examined expression at the gene level. Among these, MYL5 encodes one of the regulatory myosin light chains, a component of the motor protein myosin. MYL5 was significantly downregulated in IFN-γ-treated RA myobundles ($Log2FC = -2.316$, $P_{adj} = 1.98 \times 10^{-12}$) and to a lesser extent in controls ($Log2FC = -1.559$, $P_{adj} = 5.85 \times 10^{-8}$) (Fig. 5C). Genes with $|Log2FC| > 1$ and $p_{adj} < 0.05$ and are expressed in either IFN-γ treated RA or control myobundles relative to their corresponding untreated conditions are listed in Supplementary Data 1.

Although the primary focus of the RNA sequencing was to examine genes affected after treatment with IFN-γ, we also directly compared differential gene expression of RA myobundles to control myobundles (Supplementary Fig. 10). Since fewer genes were differentially expressed, we set a threshold of $|Log2FC| > 1$ and $p_{adj} < 0.05$. Five of the differentially expressed genes were also differentially expressed in INF-γ treated RA (AEBP1, LBP, GREM1, lncMYOD1) or control (HMCN1) myobundles relative to their corresponding untreated case (Fig. 5A and Supplementary Data 1).

Table 1 | Gene sets enriched in 7-day untreated control myobundles compared to untreated RA myobundles or IFN-γ-treated control myobundles compared to IFN-γ-treated RA myobundles

Gene Sets Enriched in untreated Control Myobundles vs. untreated RA Myobundles						
	GENE SET	Size	ES	NES	NOM p-val	FDR q-val
1	Epithelial Mesenchymal Transition[b]	200	−0.64	−1.92	<0.001	<0.001
Gene Sets Enriched in untreated RA Myobundles vs. untreated Control Myobundles						
	GENE SET	Size	ES	NES	NOM p-val	FDR q-val
1	Oxidative Phosphorylation[b]	200	0.58	1.77	<0.001	0.001
2	Hallmark Myc Targets V1[a]	200	0.49	1.52	<0.001	0.018
Gene Sets Enriched in IFN-γ treated Control Myobundles with vs. IFN-γ treated RA Myobundles						
	GENE SET	Size	ES	NES	NOM p-val	FDR q-val
1	Epithelial Mesenchymal Transition[a]	200	−0.51	−1.57	<0.001	0.04
Gene Sets Enriched in IFN-γ treated RA Myobundles vs. IFN-γ treated control Myobundles						
None						

Gene sets ordered by NES.
SIZE gene set size, *ES* enrichment score, *NES* normalized enrichment score; *NOM P-VAL* nominal *p*-value; *FDR Q-VAL* false discovery rate q-value.
[a]FDR < 0.05, NOM P-VAL < 0.05;
[b] FDR < 0.01, NOM P-VAL < 0.01

Gene set enrichment analysis. GSEA was performed using the Hallmark gene set database to compare expression datasets between RA myobundles and controls with and without IFN-γ treatment. When comparing untreated RA myobundles with untreated control myobundles, enrichment results for RA showed that of the 13 out of 50 gene sets that were upregulated, 2 gene sets—oxidative phosphorylation and MYC targets v1—were significantly enriched with an FDR < 0.05 and nominal p value < 0.05 (Table 1). For untreated controls, epithelial mesenchymal transition was the only gene set upregulated relative to untreated RA myobundles with an FDR < 0.05 and nominal p value < 0.05 (Table 1).

Compared to control myobundles treated with IFN-γ, IFN-γ-treated RA myobundles showed no significant gene set enrichment. IFN-γ-treated control myobundles showed 1 gene set that was significantly enriched: epithelial-mesenchymal transition, as was observed without IFN-γ treatment (Table 1).

Next, gene sets enriched in control myobundles treated with IFN-γ were compared to untreated control myobundles. Compared to untreated controls, IFN-γ-treated controls presented 13 statistically significant gene sets involving IFN-γ response, IFN-α response, inflammatory response, IL-6-JAK/STAT3 signaling, TNF-α signaling, apoptosis, and IL-2-JAK/STAT5 signaling (FDR < 0.05, nominal p value < 0.05) (Table 2). Untreated controls showed 1 gene set that was significantly enriched: Hallmark angiogenesis at FDR = 0.05, nominal p value < 0.05 (Table 2).

Enrichment results comparing IFN-γ-treated RA myobundles with untreated RA myobundles showed 16 statistically significant gene sets involving IFN-γ response, IFN-α response, inflammatory response, IL-6-JAK/STAT3 signaling, TNF-α signaling, apoptosis, IL2-JAK/STAT5 signaling, hypoxia, and unfolded protein response (FDR < 0.05, nominal p value < 0.05) (Table 2). Untreated RA myobundles showed no significant results. Interestingly, gene sets for hypoxia, mTOR1 signaling, and the unfolded protein response were enriched in IFN-γ-treated RA myobundles, but not IFN-γ-treated control myobundles (Table 2).

Within the gene set involving genes upregulated in response to hypoxia, only 2 genes were significantly upregulated ($|\log2FC| \geq 2$, $p_{adj} < 0.05$) in IFN-γ-treated RA myobundles but not IFN-γ-treated controls: PIM1 ($\log2FC = 2.078$; $p_{adj} = 1.17 \times 10^{-18}$) and MT-1E, an isoform of MT-1 ($\log2FC = 2.359$; $p_{adj} = 1.78 \times 10^{-12}$). Within the gene set involving genes upregulated for the MTOR1 response and the unfolded protein response, no genes were significantly upregulated in IFN-γ-treated RA myobundles or IFN-γ-treated controls.

Contractile forces and kinetics of IFN-γ-treated RA myobundles after treatment with methotrexate and tofacitinib

We next investigated whether specific therapeutics, clinically used for RA treatment, can recover RA myobundle function during continued exposure to IFN-γ after a functional deficit was produced. Given that IFN-γ targets the JAK/STAT pathway, we treated IFN-γ-treated RA myobundles with clinically relevant doses of the JAK-inhibitor tofacitinib (TOF)[27,28] or methotrexate (MTX)[29,30], the leading DMARD for RA therapy. RA myobundles were treated with 5 ng/mL IFN-γ for 7 days, from day 7 to day 14 of differentiation. After 4 days of exposure to IFN-γ, myobundles were treated with either 500 nM MTX, DMSO vehicle control for MTX, or 1 μM TOF for 3 days while also treated with IFN-γ. Endpoint testing occurred on day 14 of differentiation.

In RA myobundles, a one-way ANOVA indicated that treatment significantly affected specific twitch force ($p < 0.01$) (Fig. 6A) and specific tetanus force ($p < 0.0001$) (Fig. 6B). As expected, IFN-γ reduced specific twitch force (Fig. 6A) and specific tetanus force (Fig. 6B) in RA myobundles. In IFN-γ-treated RA myobundles, treatment with TOF fully recovered specific twitch force (Fig. 6A) and specific tetanus force (Fig. 6B). Longitudinal sections of myobundles treated with IFN-γ with or without TOF were immunostained for SAA and nuclei for one RA donor. The morphology of RA myobundles treated with TOF appeared comparable to untreated controls (Supplementary Fig. 11). MTX did not show a recovery in specific twitch or tetanus force when the results for 3 RA donors were averaged together (Fig. 6A, B).

Individual assessment of donors shows that the twitch force response was variable with 2 of 3 donors showing a response to IFN-γ (Supplementary Fig. 12A–C). For those two donors (RA108 and RA109), both showed an improvement with TOF while only RA108 showed an improvement with MTX. For tetanus, all donors responded to TOF and none of 3 RA donors exhibited full recovery of force production in response to MTX (Supplementary Fig. 12D–F).

Muscle protein analysis of IFN-γ-treated RA myobundles after tofacitinib treatment

Western blot for MYH and MYL were compared to a β-actin control for 3 RA donors. In RA myobundles compared to untreated controls, IFN-γ treatment showed a trend towards reduced but not significant MYH levels in RA myobundles, which increased significantly after treatment with TOF (Fig. 7A, B). MYL levels in RA myobundles were unaffected by IFN-γ treatment with or without TOF (Fig. 7A, C).

Table 2 | Gene sets enriched in 7-day IFN-γ-treated control myobundles compared to untreated control myobundles or IFN-γ-treated RA myobundles compared to untreated RA myobundles

Gene Sets Enriched in IFN-γ-treated Control Myobundles vs. Untreated Control Myobundles						
	GENE SET	**Size**	**ES**	NES	NOM p-val	FDR q-val
1	Interferon Gamma Response[b]	199	0.91	2.64	<0.001	<0.001
2	Interferon Alpha Response[b]	97	0.95	2.55	<0.001	<0.001
3	Allograft Rejection[b]	200	0.73	2.12	<0.001	<0.001
4	Inflammatory Response[b]	200	0.69	2.01	<0.001	<0.001
5	IL-6 JAK/STAT3 Signaling[b]	87	0.76	2.00	<0.001	<0.001
6	TNF-α Signaling Via NfκB[b]	199	0.64	1.87	<0.001	<0.001
7	Complement[b]	200	0.62	1.80	<0.001	<0.001
8	Cholesterol Homeostasis[a]	74	0.59	1.53	0.008	0.015
9	P53 Pathway[a]	200	0.52	1.52	<0.001	0.014
10	Apoptosis[a]	160	0.53	1.51	<0.001	0.015
11	UV Response Up[a]	157	0.52	1.48	0.001	0.020
12	IL2 Stat5 Signaling[a]	199	0.49	1.42	0.003	0.036
13	Androgen Response[a]	100	0.52	1.39	0.020	0.049
14	Hypoxia	200	0.46	1.34	0.010	0.081
Gene Sets Enriched in IFN-γ-treated RA Myobundles vs. Untreated RA Myobundles						
	GENE SET	Size	ES	NES	NOM p-val	FDR q-val
1	Interferon Gamma Response[b]	199	0.90	2.60	<0.001	<0.001
2	Interferon Alpha Response[b]	197	0.94	2.51	<0.001	<0.001
3	Allograft Rejection[b]	200	0.73	2.13	<0.001	<0.001
4	Inflammatory Response[b]	200	0.71	2.08	<0.001	<0.001
5	IL-6 JAK/STAT3 Signaling[b]	87	0.78	2.05	<0.001	<0.001
6	TNF-α Signaling Via NFκB[b]	99	0.68	1.99	<0.001	<0.001
7	Complement[b]	200	0.65	1.89	<0.001	<0.001
8	Apoptosis[b]	160	0.60	1.71	<0.001	<0.001
9	P53 Pathway[a]	200	0.57	1.64	<0.001	0.002
10	IL2 Stat5 Signaling[a]	199	0.56	1.61	<0.001	0.002
11	UV response Up[a]	157	0.55	1.55	<0.001	0.006
12	Androgen response[a]	100	0.57	1.51	0.003	0.011
13	Hypoxia[b,c]	200	0.52	1.51	<0.001	0.011
14	Cholesterol homeostasis[a]	74	0.55	1.41	0.028	0.032
15	MTOR1 Signaling[a,c]	200	0.48	1.39	0.004	0.037
16	Unfolded protein response[a,c]	113	0.51	1.36	0.022	0.049
Gene Sets Enriched in Untreated Control Myobundles vs. IFN-γ-treated Control Myobundles						
	GENE SET	Size	ES	NES	NOM p-val	FDR q-val
1	Hallmark Angiogenesis	36	0.62	1.50	0.012	0.050
Gene Sets Enriched in Untreated RA Myobundles vs. IFN-γ-treated RA Myobundles						
None						

Gene sets ordered by NES.
SIZE gene set size, *ES* enrichment score, *NES* normalized enrichment score, *NOM P-VAL* nominal p-value, *FDR Q-VAL* false discovery rate q-value.
[a]FDR < 0.05, NOM P-VAL < 0.05.
[b]FDR < 0.01, NOM P-VAL < 0.01.
[c]The gene set is enriched in IFN-γ-treated RA myobundles but not IFN-γ-treated controls at FDR < 0.05, NOM P-VAL < 0.05.

PIM1 protein expression after treatment of RA myobundles with IFN-γ with and without tofacitinib

A consistent finding from RNA sequencing was elevation of PIM1 and MT-1E after IFN-γ treatment in RA myobundles but not control myobundles. To assess whether this led to altered protein expression which could be restored by tofacitinib treatment, Western blots for PIM1 were performed with the same samples used to measure MYH and MYL (Fig. 7D). Quantification of band intensities indicated that PIM1 levels increased after treatment with 5 ng/mL IFN-γ for 7 days but did not change if 1 μM tofacitinib was added with the IFN-γ (Fig. 7E). We did not observe expression of MT-1E by Western blot.

Inflammatory marker expression in IFN-γ-treated RA myobundles after treatment with methotrexate and tofacitinib

To examine how inflammatory factors relevant to RA pathology were influenced in RA myobundles by exposure to IFN-γ with and without treatment with MTX or TOF, we assessed expression of genes IFN-γ, IL-1β, IL-6, and TNF-α for 3 RA donors. Although not statistically

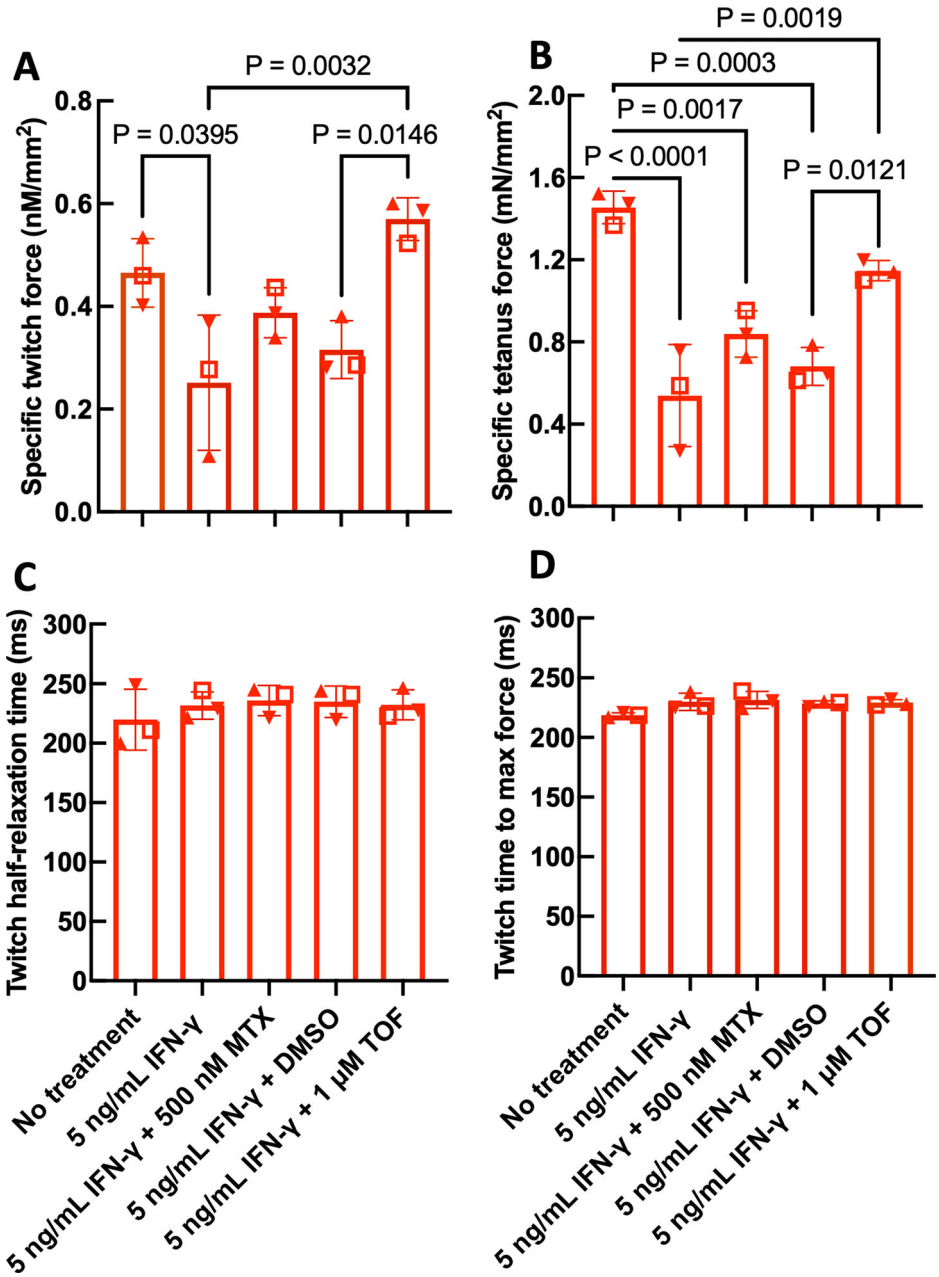

Fig. 6 | Contractile forces and kinetics of IFN-γ-treated RA myobundles after treatment with methotrexate or tofacitinib. A Specific twitch force, (**B**) specific tetanus force, (**C**) twitch time to max force, and (**D**) twitch half-relaxation time of RA myobundles treated with IFN-γ for 7 days with or without MTX or TOF for 3 days, and force tested on day 14 of differentiation. $N = 3$ RA donors (RA107 (▼), RA108 (□), RA109(▲)); twitch force and kinetics, $n = 4–7$ myobundles; tetanus force, $n = 3–7$ myobundles. Data are represented as mean ± S.D. and analyzed one-way ANOVA followed by Tukey HSD post-hoc test.

significant, there was a trend for upregulated IFN-γ and IL-1β expression in response to IFN-γ treatment, and a trend for downregulated IFN-γ and IL-1β expression when treated with TOF (Fig. 8A, B). IFN-γ significantly upregulated IL-6 expression in RA myobundles (Fig. 8C). MTX and TOF each restored IL-6 expression levels to baseline (Fig. 8C). Although not statistically significant, TNF-α showed a trend of upregulated expression with IFN-γ treatment (Fig. 8D). TOF downregulated TNF-α expression to levels comparable to untreated controls (Fig. 8D).

Discussion

Compared to healthy controls, RA myobundles were more sensitive to 5 ng/mL IFN-γ resulting in reduced force production. RA and control myobundles did not respond to treatment with IL-6 for the times and doses examined. Gene sets that were enriched in IFN-γ-treated RA myobundles, but not IFN-γ-treated controls, involved genes upregulated in response to hypoxia, MTOR1 signaling, and the unfolded protein response. From the hypoxia gene set, PIM1 and MT-1E were identified as potential therapeutic targets for treating RA-associated muscle dysfunction. Treatment with tofacitinib fully restored contractile force and myosin heavy chain and PIM1 protein levels in RA myobundles with IFN-γ-induced dysfunction, whereas methotrexate was less effective.

There may be several explanations as to why IL-6 did not significantly affect RA myobundles or controls. Since we focused on differential effects between RA and control myobundles, the IL-6 concentration may have been too low or the treatment duration not long enough to induce an effect. Low levels of soluble IL-6 receptor or gp130 receptor in our myobundles may limit uptake of the IL-6 protein by the myobundles. While in circulation, IL-6 can bind to the soluble IL-6 receptor becoming an IL-6/sIL-6R complex. All cells in the body express gp130, whereas membrane-bound IL-6R is primarily expressed by hepatocytes and immune cells[31]. Thus, unlike IL-6, the IL-6/sIL-6R complex binds to and stimulates cells expressing gp130[31]. In classical signaling, IL-6 binds to the membrane-bound IL-6R forming the IL-6/IL-6R complex. The formation of this complex induces gp130 activation resulting in signal transduction[31]. Soluble IL-6R levels were ~2 times

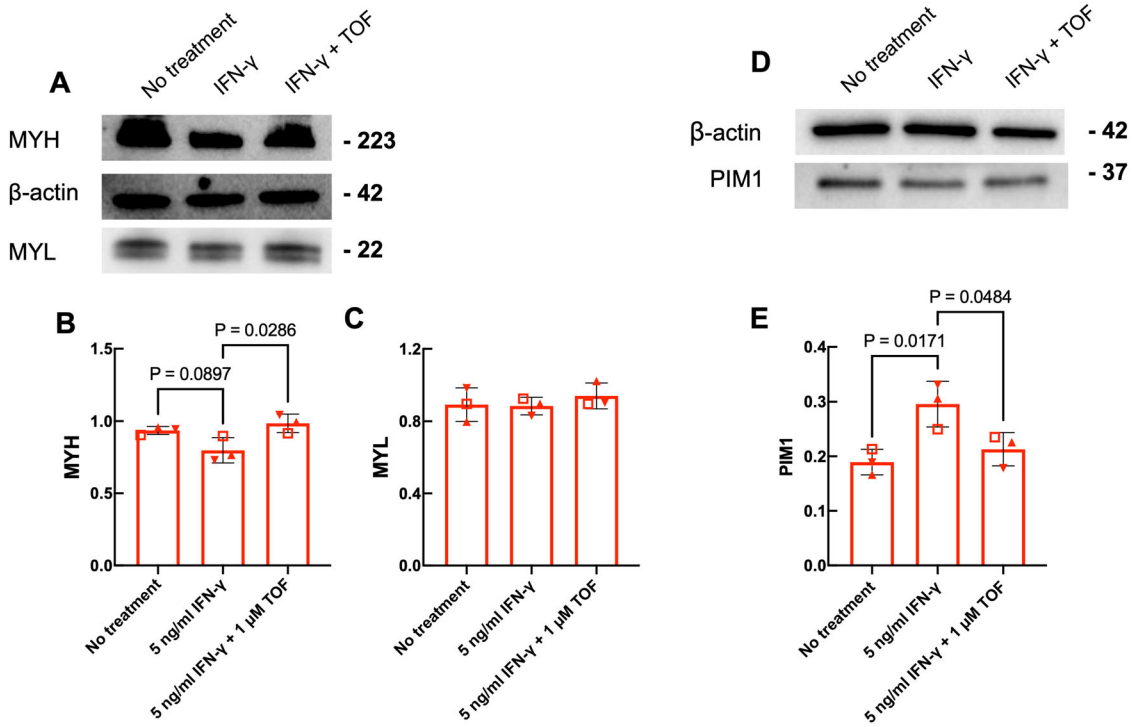

Fig. 7 | Western blot of contractile proteins in IFN-γ-treated RA myobundles after treatment with tofacitinib. A Western blot of MYH and MYL in one RA donor on day 14 of differentiation after 7 days of IFN-γ treatment with or without TOF for 3 days. Quantified expression of (**B**) MYH and (**C**) MYL normalized to β-actin. $N = 3$ RA donors (RA107 (▼), RA108 (□), RA109 (▲)). 4 myobundles were pooled together per condition per donor to obtain protein sample. Data are represented as mean ± S.D. and analyzed using one-way ANOVA, followed by Tukey HSD post-hoc test. **D** Western blot of PIM1 protein in IFN-γ-treated RA myobundles after treatment with tofacitinib. **E** Quantified expression of PIM1 normalized to β-actin.

greater in untreated controls compared to untreated RA myobundles (Fig. 3C). The higher IL-6 receptor levels in controls may explain why trends of positive effects were observed in IL-6-treated controls but not IL-6-treated RA myobundles.

Gene sets that were enriched in IFN-γ-treated RA myobundles, but not IFN-γ-treated controls, involved genes upregulated (1) in response to hypoxia, (2) related to MTOR1 signaling, and (3) protein misfolding in the endoplasmic reticulum (unfolded protein response). In skeletal muscle, oxygen plays a critical role in metabolic signaling, energy production, and regulation of intercellular pathways which alter proliferation, differentiation, and survival of myogenic cells[32]. Hypoxia occurs during pathological conditions including RA and inhibits the differentiation of myoblasts[32,33]. Within the gene set involving response to hypoxia, 2 genes were found to be significantly upregulated ($|\log2FC| \geq 2$, adjusted p value < 0.05) in IFN-γ-treated RA myobundles but not IFN-γ-treated controls: PIM1 and MT-1E.

PIM kinases have been implicated as important factors in cellular stress and show increased expression in hypoxia[34]. PIM1, a PIM isoform, is a direct target gene of the JAK/STAT signaling pathway and is involved in immune regulation and inflammatory response[35]. Pro-inflammatory factors such as IL-1β, IL-6, and IL-8 enhance PIM1 expression, and inhibition of PIM1 reduces production of inflammatory cytokines and chemokines[35–37]. Pim1 kinase is a positive regulator of myoblast behavior in vitro and muscle regeneration in vivo in mice[35]. In our RA myobundle model, PIM1 upregulation after IFN-γ treatment was likely caused by activation of JAK/STAT signaling by IFN-γ. Initial upregulation of PIM1 may promote muscle regeneration as a recovery response to IFN-γ-induced muscle dysfunction. However, sustained PIM1 activity may contribute to a prolonged inflammatory response, exacerbating muscle dysfunction in RA. Given the observed changes of PIM1protein in IFN-γ-treated RA myobundles with and without tofacitinib treatment (Fig. 7E), further investigation into PIM1 as a potential therapeutic target for skeletal muscle injury is warranted.

Although RNA-seq indicated that MT-1E was a potential target, we did not observe MT-1E by western blot, even at low dilution (1:100). Although Western blot failed to show consistent effects of RA disease or cytokine treatment on myosin light or heavy chains proteins using antibodies that recognized all isoforms of these proteins, RNA-seq did show that MYL5 was significantly reduced just in RA myobundles exposed to 5 ng/ml IFN-γ.

Skeletal muscle has a specialized endoplasmic reticulum (ER) called the sarcoplasmic reticulum. The ER is involved in protein folding and trafficking within the cell and regulates calcium ion release into the cytoplasm to initiate muscle contraction[38]. Under hypoxic conditions, ER homeostasis is disrupted resulting in accumulation of misfolded and unfolded proteins in the ER[38]. This leads to ER stress and activation of the unfolded protein response[38]. The unfolded protein response is upregulated in skeletal muscle under catabolic states associated with cachexia, sarcopenia, inflammatory myopathies, and aging[38–40]. Further, this stress may affect autophagy which is consistent with increased MTOR1 signaling. Additionally, ROS production and oxidative stress may be associated with ER stress and the unfolded protein response[41].

Treatment with a clinically relevant dose of JAK inhibitor TOF successfully restored contractile function in RA myobundles with IFN-γ-induced deficit and downregulated IL-6 and TNF-α expression to baseline levels. These results are supported by previous clinical studies in which patients were treated with tofacitinib[42]. Over the course of treatment, patient serum levels of TNF-α, IL-6, and IFN-γ were significantly reduced[42].

Although MTX is often the first-line medication for RA treatment, its effects on skeletal muscle are not well understood compared to other cell types. Methotrexate inhibits the pro-inflammatory properties of immune cells, endothelial cells, and fibroblast-like synoviocytes involved in RA pathogenesis through a variety of different mechanisms[19,20]. Methotrexate alters purine and pyrimidine metabolism which reduces T cell proliferation, inhibits transmethylation reactions which prevent T cell cytotoxicity, interferes with glutathione metabolism alters recruitment of immune cells, promotion of adenosine release which

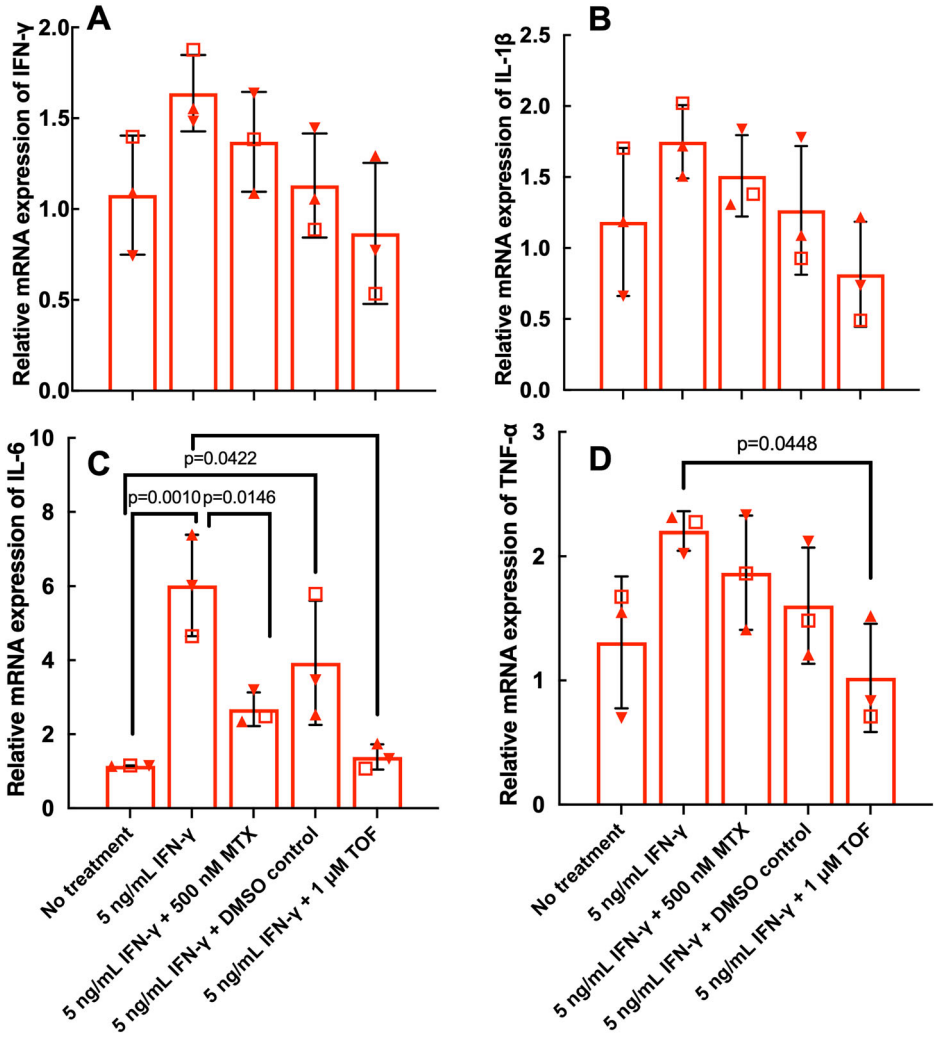

Fig. 8 | Gene expression of IFN-γ-treated RA myobundles after treatment with methotrexate or tofacitinib. RA myobundles were treated with IFN-γ for 7 days with or without MTX or TOF for 3 days, and flash frozen on day 14 of differentiation. Quantified gene expression of (**A**) IFN-γ, (**B**) IL-1β, (**C**) IL-6, and (**D**) TNF-α normalized to GAPDH. $N = 3$ RA donors (RA107 (▼), RA108 (□), RA109 (▲), $n = 3$ myobundles per donor. Data are represented as mean ± S.D. and analyzed using one-way ANOVA, followed by Tukey HSD post-hoc test.

mediates inflammation, and reduction of reactive oxygen groups in the synoviocytes of RA patients[19–21].

In our work, MTX was tested in IFN-γ-treated RA myobundles generated from 3 donors. When the results for the 3 RA donors were averaged together, MTX did not show a recovery effect (Fig. 6). Although two of the three RA donors did not show a significant response to treatment with MTX, one donor exhibited full recovery of force production (Supplementary Fig. 12). These variable results indicate response to MTX treatment may be donor-dependent, highlighting the potential of RA-patient-derived myobundles to serve as a method to tailor drug therapy for individual patients. Overall, our findings indicate the suitability of our model for studies of RA-associated muscle dysfunction and therapy.

Since IFN-γ is not traditionally a key player in RA, our model would benefit from the addition of other key pro-inflammatory cytokines associated with RA pathology, such as TNF-α. TNF-α is elevated in RA serum (17.9 pg/mL) compared to healthy controls (5.5 pg/mL)[43]. Preliminary experiments (Supplementary Fig. 1) showed that a 3-day exposure to 5 ng/mL TNF-α did not affect RA contractile force, chronic TNF-α elevation is associated with muscle wasting and loss of muscle function[44,45]. TNF-α enhances protein catabolism[46], decreases muscle contractile force, and leads to increased production of muscle-derived oxidants[47,48]. In cultured murine skeletal muscle, TNF-α impairs myoblast cell cycle exit and suppresses MyoD gene and protein expression[49,50], thereby inhibiting muscle cell fusion and differentiation into mature fibers. TNF-α may decrease the force of mature fibers by altering Ca2+ release from the sarcoplasmic reticulum[51]. Although predominantly generated by immune cells in response to antigenic challenges and cancer, TNF-α is produced by skeletal muscle[52]. Thus, chronic inflammation in RA can create a positive feedback loop in which TNF-α secretion by skeletal muscle exacerbates the inflammatory response, further weakening the muscle tissue.

Since chronic inflammation and muscle loss are important in osteoarthritis, sarcopenia, and cachexia[53], this work serves as a proof-of-principal for modeling and treating inflammation of muscle that can be applied to diseases beyond RA. Sarcopenia is a primary example of an additional application of our work. Sarcopenia is a loss of muscle mass and function in the elderly that reduces mobility and quality of life[54] and is associated with increased levels of pro-inflammatory cytokine IL-6, anti-inflammatory cytokine IL-10, and IL-6/IL-10 ratios[54,55]. Myostatin may also play an important role in sarcopenia[56–58]. Myobundles generated from aged healthy cells show low contractile function and produce cytokines IL-6 and IL-10, as described in previous work[24]. Such aged healthy myobundles could provide the basis for a model of sarcopenia and could be validated by comparing them to myobundles generated from muscle cells of sarcopenia donors. A myobundle model of sarcopenia would provide a platform to test the efficacy of pharmacologic agents to improve muscle function in patients with sarcopenia. This model could be used to test myostatin inhibitors FDA-approved for sarcopenia treatment, such as trevogrumab[59], as well as novel therapeutic approaches including inhibitors of IL-6, such as the RA therapeutic tocilizumab[60].

The ability to generate and couple together multiple tissue organs will allow for the study of organ-organ crosstalk in a tightly regulated environment and provide more physiologically relevant drug screens capable of identifying drug toxicity across multiple tissue types. Future work will involve integrating our RA myobundles with human tissue-engineered

blood vessels (TEBVs) thus expanding the relevance of our model to RA pathology involving the cardiovascular system. Given cardiovascular disease, including atherosclerosis, is a major co-morbidity associated with RA[61], the field could benefit from an integrated myobundle-TEBV microphysiological system to elucidate mechanisms of disease progression and test drug safety and efficacy across tissue types.

Methods

Selection of RA donors and age-matched controls

This study was approved by the Duke University Institutional Review Board and complied with the Helsinki Declaration. Participants provided informed consent to provide a muscle biopsy. Individuals with RA and age-matched controls, ages 55-85, were selected within Durham, NC, as previously described in ref. 24. RA donors met the following criteria: (1) RA diagnosis meeting American College of Rheumatology 2010 criteria[62]; (2) positive rheumatoid factor or anti-citrullinated protein antibody or erosions typical of RA on radiographs; (3) prednisone use of less than or equal to 5 mg per day; (4) no pharmacologic therapy with corticosteroids within the 3 weeks prior to study enrollment; and (5) a score of 5 or above on the following phone screen question: "On a scale of 1 to 10, how severe would you rate your RA disease? 1 = 'I can't tell I have RA' and 10 = 'I have multiple joints that are stiff and swollen and my RA is as bad as it has ever been.' " The disease activity score in 28 joints (DAS28) was determined using a patient-completed visual analog scale (VAS), physician-determined numbers of tender and swollen joints, and erythrocyte sedimentation rate (ESR)[63]. Healthy participants, who did not have a diagnosis of RA, were matched to individual participants with RA by gender and age within 3 years. Exclusions from the study included: (1) current use of ticlopidine, clopidogrel, dipyridamole, warfarin, heparin, enoxaparin and other blood thinners; (2) current use of biologic agents, except those targeting TNF-α; (3) other inflammatory arthropathy or myopathy, Paget's disease, pigmented villonodular synovitis, joint infection, ochronosis, neuropathic arthropathy, osteochondromatosis, acromegaly, hemochromatosis, Wilson's disease, osteonecrosis, or knee replacement within the last three months; (4) diagnosis of active malignancy, congestive heart failure, diabetes mellitus or chronic obstructive pulmonary disease; and (5) coronary stents or any other medical condition for which aspirin cannot be temporarily withheld.

Human myoblast culture

Human skeletal muscle cells were isolated from *vastus lateralis* biopsy samples and cultured as previously described[23–25]. Briefly, myoblasts were cultured in human growth media (hGM) containing low-glucose (LG; 1 g/L glucose) DMEM (Gibco), 8% fetal bovine serum (Hyclone), 0.4 μg/mL Dexamethasone (Sigma), 10 ng/mL EGF (VWR), 50 μg/mL Fetuin (Sigma), 0.1% Gentamycin (1x) (Gibco), 0.1% Amphotericin B (1x) (Gibco). At ~80% confluence, myoblasts were enzymatically removed from the flask with 0.05% trypsin-EDTA and used to generate three-dimensional myobundles.

Human myobundle culture and treatment

Myobundles were fabricated and cultured as previously described[23–25]. Briefly, A well-mixed cell solution (7.5×10^5 cells in 17.2 μL media and 2 μL of 50 U/mL thrombin in 0.1% BSA in PBS per bundle) was added to an ice-cold gelling solution (11 μL media, 10 μL Matrigel, and 10 μL of 20 mg/mL fibrinogen in DMEM). The mixture was pipetted in a custom-made Teflon mold placed between two ends of a nylon (Cerex Advanced Fabrics) frame. myobundles were polymerized in the mold and to the frame for 30 min and then cultured in hGM containing 1.5 mg/mL 6-aminocaproic acid (ACA) on a rocker (0.33 Hz) at 37 °C. On day 4, the media was switched to differentiation media (hDM) consisting of LG-DMEM supplemented with 1X N-2 supplement (ThermoFisher Scientific), 0.1% gentamycin (1x), 0.1% amphotericin B (1x), and 2 mg/mL of ACA.

Beginning on day 7 of differentiation, myobundles were treated with 5 ng/mL IFN-γ (PeproTech, 300-02) for 4 days with or without 5 ng/mL IL-6. Next, myobundles were treated for 3 days with 5 ng/mL IFN-γ and either 500 nM methotrexate (MTX) (in DMSO; Sigma–Aldrich, A6770) or 1 μM tofacitinib (TOF) (in water; Sigma–Aldrich, PZ0017). Myobundles were differentiated for up to 14 days. Media was changed every other day.

Contractile function and kinetics measurements

Myobundles were stretched to 115% of normal length using a custom-made force measurement setup as previously described[23,24] and then stimulated at 1 Hz for 1 s to obtain twitch force (single pulse), at 20 Hz for 1 s to obtain tetanus force, and at 20 Hz for 30 s to obtain fatigue force. Peak twitch and tetanus force, percent fatigue, and twitch kinetics (time to peak twitch and half-relaxation time) were calculated using a Matlab script. Twitch and tetanus forces were calculated as the difference between the highest measured force after stimulation and the baseline passive force prior to stimulation. Specific twitch and tetanus forces were obtained by dividing the force output of a myobundle by the myobundle cross-sectional area. Images were taken of the myobundles prior to force testing and Image J was used to determine the diameter at the mid-point of each bundle. Myobundle cross-sectional area was calculated under the assumption that each myobundle cross-section is a perfect circle. Fatigue represents the force after 30 s divided by the difference between the peak force and the baseline force. Twitch time to maximum force was determined as the time between onset of electrical stimulation and peak force. Twitch half-relaxation time was calculated as the time between peak force and return to one-half of the difference between the peak force and the baseline force.

Immunofluorescence staining of myobundles

Sample preparation and immunostaining were performed as previously described[23,24]. Briefly, myobundles were fixed using 4% PFA for 1.5 h at room temperature and then rinsed three times with DPBS containing calcium and magnesium. Myobundles were embedded in OCT compound, flash frozen in liquid nitrogen, and sectioned on a cryotome (Leica CM3050, 10 μm thickness). Myobundle sections were permeabilized with 0.1% Triton X for 30 min at room temperature and washed 2 times for 5 min in PBS. After incubating sections in blocking buffer for at least 2 h at 4 °C primary antibodies for sarcomeric α-actinin (SAA) (Abcam, ab9465, 1:200) in blocking buffer was added for 24 h at 4 °C. Sections were rinsed three times with blocking buffer and incubated with fluorescently labeled goat anti-mouse secondary antibody (Invitrogen, A11029, 1:250) and Hoechst 33342 (Invitrogen, H3570, 1:1000) in blocking buffer for 2 h at room temperature. Sections were then rinsed three times in PBS and mounted under a coverslip using Fluoromount-G. Samples were imaged at 20x and 40x magnification using a Zeiss LSM 510 inverted confocal microscope and the NIS Elements software. Images of myobundle cross-sections and longitudinal sections were quantified using ImageJ. The number of nuclei in the sections was identified from Hoechst staining and counted. the fraction associated with sarcomeric α-actinin+ cells showing straited recorded as the percentage of nuclei in striated fibers.

Western blotting

Myobundle protein was isolated in RIPA lysis and extraction buffer with protease and phosphatase inhibitor cocktail (Thermo Scientific). Protein concentration was determined using Precision Red assay (Cytoskeleton, Inc., Denver, CO) according to the manufacturer's instructions. Western blot was performed using Bio-Rad 4–15% Mini-PROTEAN protein gels (Bio-Rad, Hercules, CA). The following primary antibodies were used for detection: beta-actin loading control (Invitrogen, MA5-15739, 1:1000), myosin heavy chain (MYH) (DSHB, AB_2147781 or MF20, 1:200), CD126/IL-6R (Bio-Rad, AHP2449, 1:500), myosin light chain (MYL) (SCBT, sc-365243, 1:1000), PIM1 (Invitrogen, 39-4600, 1:100 and 1:500), and MT-1E (Invitrogen, MA5-43655, 1:100, 1:250 and 1:500). HRP conjugated anti-mouse antibody (1:2000) was purchased from Invitrogen (#626520). HRP conjugated anti-rabbit antibody (1:5000) was purchased from Vector Laboratories (PI-1000-1). Chemiluminescence was performed using West Femto Maximum Sensitivity Substrate (Thermo Scientific, 34095) for IL-6R detection and Clarity Western ECL substrate (Bio-Rad, 1705061) for

detection of all other proteins. Images were acquired using a Bio-Rad ChemiDoc imaging system and analyzed using the rolling ball average method in ImageJ.

RNA-sequencing

RA and control myobundles were flash frozen in liquid nitrogen on day 14 of differentiation prior to total RNA extraction. Samples were stored at −80 °C until assayed. RNA extraction was performed using the Aurum Total RNA Mini Kit from BioRAD. RNA libraries were sequenced as 50 pair-ended base pairs with a NovaSeq 6000 S-Prime (sequencing output per flow cell: 65–80 Gb; clusters passing filter per flow cell: 650–800 M) at the Duke Sequencing and Genomics Technologies Core Facility. RNA-seq data was processed using the TrimGalore toolkit (https://www.bioinformatics.babraham.ac.uk/projects/trim_galore/) which employs Cutadapt[64] to trim low-quality bases and Illumina sequencing adapters from the 3′ end of the reads. Only reads longer than 20 nt after trimming were maintained further analysis. Reads were mapped to the GRCh38v93 version of the human genome and transcriptome (http://www.ensembl.org) using the STAR RNA-seq alignment tool (http://www-huber.embl.de/users/anders/HTSeq/)[65]. Reads were kept for subsequent analysis if they mapped to a single genomic location. Gene counts were compiled using the HTSeq tool[66]. Only genes that had at least 10 reads in any given library were used in subsequent analysis. Normalization and differential expression were carried out using the DESeq2[67] Bioconductor[68] package with the R statistical package (www.r-project.org) and individual donors were included as a cofactor in the model. The false discovery rate was calculated to control for multiple hypothesis testing. Gene set enrichment analysis (GSEA) and QIAGEN IPA[69,70] were performed to identify gene ontology terms and pathways associated with altered gene expression for each of the comparisons performed. GSEA was conducted using Hallmark gene set database (and human Ensembl gene IDs) with an FDR cutoff of 0.05 and nominal p value of 0.05 or less. Volcano plots and Venn diagrams of differentially expressed genes were generated using Python. When generating these plots, cutoff criteria were implemented in which the adjusted p value was 0.05 or less and log2FC was the absolute value of 2 or greater. RNA sequencing files are deposited at NCBI GEO (accession number # GSE283881).

Quantitative RT-PCR

RA myobundles were flash-frozen in liquid nitrogen on day 14 of differentiation prior to total RNA extraction. RNA extraction was performed using the Aurum Total RNA Mini Kit (BioRAD). The iScript cDNA Synthesis Kit from BioRad was used to produce cDNA. Genes of interest IFN-γ, IL-1β, IL-6, TNF-α, and housekeeping gene GAPDH were amplified and quantified using the iQ SYBR Supermix (BioRad) and CFX Connect Real-Time Detection System (BioRad). Primer sequences are listed in Supplementary Table 2.

Statistical analysis

For experiments involving multiple donors, a global normalization method was used for each functional measure to account for inherent variability between myobundles generated from different donors. To account for this variation among donors, we first calculated a global average of the response over all donors and all treatments,

$$\bar{Y} = \frac{1}{nm}\sum_{j}^{m}\sum_{i=1}^{n} Y_{i,j} \quad (1)$$

Where m is the number of replicates per donor and n is the number of donors. Next, we compute the average response per donor for all treatments,

$$\bar{Y}_j = \frac{1}{n}\sum_{i=1}^{n} Y_{i,j} \quad (2)$$

Then each donor j is multiplied by the weighting factor $\frac{\bar{Y}}{\bar{Y}_j}$. If the donor average is below the global average, the weighting factor increases the magnitude of the responses for that donor and if the donor average is above the global average, the weighting factor reduces the response for that donor. The global average is unchanged. Applying normalization for donor averages isolates the effect of the treatment. Examination of the two-way analysis of variance indicated that global normalization greatly reduced the error sum of squares but had a modest effect (1% change) on the model sum of squares. Global normalization maintains the relative differences between conditions within donors while minimizing differences between donors.

For experiments involving multiple donors, individual donor averages were used for statistical analysis and the number of donors was used to determine the standard deviation (S.D.). For experiments involving one donor, individual myobundle output values were used for statistical analysis and the number of myobundles per condition was used to determine S.E.M. Results were compared using JMP (SAS) with a one-way or two-way ANOVA followed by a post-Hoc Tukey test for multiple comparisons.

Reporting summary

Further information on research design is available in Nature Portfolio Reporting Summary linked to this article.

Data availability

The RNA sequencing files are available at NCBI GEO (accession number # GSE283881). Supplementary Figs. 13–16 include the uncropped and unedited images of the blots used in Figs. 3A, 7A, D, and Supplementary Fig. 7. Numerical source data for all figures is provided in Supplementary Data 2, 3.

Code availability

The MATLAB code used to obtain the twitch and kinetic parameters for the myobundles is available upon request.

Received: 17 June 2022; Accepted: 20 March 2025;
Published online: 09 April 2025

References

1. Jacobs, P., Bissonnette, R. & Guenther, L. C. Socioeconomic burden of immune-mediated inflammatory diseases—focusing on work productivity and disability. *J. Rheumatol. Suppl.* **88**, 55–61 (2011).
2. Choy, E. Understanding the dynamics: pathways involved in the pathogenesis of rheumatoid arthritis. *Rheumatology* **51**, v3–v11 (2012).
3. Scott, D. L., Wolfe, F. & Huizinga, T. W. Rheumatoid arthritis. *Lancet* **376**, 1094–1108 (2010).
4. Baker, J. F. et al. Assessment of muscle mass relative to fat mass and associations with physical functioning in rheumatoid arthritis. *Rheumatology***56**, 981–988 (2017).
5. Aguila, L. A. et al. Clinical and laboratory features of overlap syndromes of idiopathic inflammatory myopathies associated with systemic lupus erythematosus, systemic sclerosis, or rheumatoid arthritis. *Clin. Rheumatol.* **33**, 1093–1098 (2014).
6. Kramer, H. R., Fontaine, K. R., Bathon, J. M. & Giles, J. T. Muscle density in rheumatoid arthritis: associations with disease features and functional outcomes. *Arthritis Rheum.* **64**, 2438–2450 (2012).
7. Lemmey, A. B. et al. Tight control of disease activity fails to improve body composition or physical function in rheumatoid arthritis patients. *Rheumatology* **55**, 1736–1745 (2016).
8. Roubenoff, R. Sarcopenic obesity: does muscle loss cause fat gain? Lessons from rheumatoid arthritis and osteoarthritis. *Ann. N.Y. Acad. Sci.* **904**, 553–557 (2000).
9. Roubenoff, R. Rheumatoid cachexia: a complication of rheumatoid arthritis moves into the 21st century. *Arthritis Res. Ther.* **11**, 108 (2009).
10. Giles, J. T. et al. Abnormal body composition phenotypes in older rheumatoid arthritis patients: association with disease characteristics and pharmacotherapies. *Arthritis Rheum.* **59**, 807–815 (2008).

11. Hakkinen, A. et al. Muscle strength, pain, and disease activity explain individual subdimensions of the Health Assessment Questionnaire disability index, especially in women with rheumatoid arthritis. *Ann. Rheum. Dis.* **65**, 30–34 (2006).
12. Ekdahl, C. & Broman, G. Muscle strength, endurance, and aerobic capacity in rheumatoid arthritis: a comparative study with healthy subjects. *Ann. Rheum. Dis.* **51**, 35–40 (1992).
13. Rall, L. C. et al. Protein metabolism in rheumatoid arthritis and aging. Effects of muscle strength training and tumor necrosis factor alpha. *Arthritis Rheum.* **39**, 1115–1124 (1996).
14. Huffman, K. M. et al. Molecular alterations in skeletal muscle in rheumatoid arthritis are related to disease activity, physical inactivity, and disability. *Arthritis Res. Therapy* **19**, https://doi.org/10.1186/s13075-016-1215-7 (2017).
15. Yoshida, Y. & Tanaka, T. Interleukin 6 and rheumatoid arthritis. *Biomed. Res. Int.* **2014**, 698313 (2014).
16. Jones, S. A. et al. Interleukin 6: the biology behind the therapy. *Consid. Med.* **2**, 2–6 (2018).
17. Munoz-Canoves, P., Scheele, C., Pedersen, B. K. & Serrano, A. L. Interleukin-6 myokine signaling in skeletal muscle: a double-edged sword?. *FEBS J.* **280**, 4131–4148 (2013).
18. Barrat, F. J., Crow, M. K. & Ivashkiv, L. B. Interferon target-gene expression and epigenomic signatures in health and disease. *Nat. Immunol.* **20**, 1574–1583 (2019).
19. Cronstein, B. N. Low-dose methotrexate: a mainstay in the treatment of rheumatoid arthritis. *Pharmacol. Rev.* **57**, 163–172 (2005).
20. Cronstein, B. N. & Aune, T. M. Methotrexate and its mechanisms of action in inflammatory arthritis. *Nat. Rev. Rheumatol.* **16**, 145–154 (2020).
21. Ollewagen, T., Myburgh, K. H., van de Vyver, M. & Smith, C. Rheumatoid cachexia: the underappreciated role of myoblast, macrophage and fibroblast interplay in the skeletal muscle niche. *J. Biomed. Sci.* **28**, 15 (2021).
22. Harrington, R., Al Nokhatha, S. A. & Conway, R. J. A. K. Inhibitors in rheumatoid arthritis: an evidence-based review on the emerging clinical data. *J. Inflamm. Res.* **13**, 519–531 (2020).
23. Madden, L., Juhas, M., Kraus, W. E., Truskey, G. A. & Bursac, N. Bioengineered human myobundles mimic clinical responses of skeletal muscle to drugs. *eLife* **4**, https://doi.org/10.7554/eLife.04885 (2015).
24. Oliver, C. E. et al. Tissue engineered skeletal muscle model of rheumatoid arthritis using human primary skeletal muscle cells. *J. Tissue Eng. Regen. Med.* **16**, 128–139 (2022).
25. Cheng, C. S., Ran, L., Bursac, N., Kraus, W. E. & Truskey, G. A. Cell density and joint microRNA-133a and microRNA-696 inhibition enhance differentiation and contractile function of engineered human skeletal muscle tissues. *Tissue Eng. Part A* **22**, 573–583 (2016).
26. Khodabukus, A. et al. Electrical stimulation increases hypertrophy and metabolic flux in tissue-engineered human skeletal muscle. *Biomaterials* **198**, 259–269 (2019).
27. Sandborn, W. J. et al. Tofacitinib, an oral Janus kinase inhibitor, in active ulcerative colitis. *N. Engl. J. Med.* **367**, 616–624 (2012).
28. Chen, Z., Li, B., Zhan, R. Z., Rao, L. & Bursac, N. Exercise mimetics and JAK inhibition attenuate IFN-gamma-induced wasting in engineered human skeletal muscle. *Sci. Adv.* **7**, https://doi.org/10.1126/sciadv.abd9502 (2021).
29. Bannwarth, B., Pehourcq, F., Schaeverbeke, T. & Dehais, J. Clinical pharmacokinetics of low-dose pulse methotrexate in rheumatoid arthritis. *Clin. Pharmacokinet.* **30**, 194–210 (1996).
30. Lucas, C. J., Dimmitt, S. B. & Martin, J. H. Optimising low-dose methotrexate for rheumatoid arthritis-A review. *Br. J. Clin. Pharmacol.* **85**, 2228–2234 (2019).
31. Villar-Fincheira, P. et al. Role of interleukin-6 in vascular health and disease. *Front. Mol. Biosci.* **8**, 641734 (2021).
32. Pircher, T. et al. Hypoxic signaling in skeletal muscle maintenance and regeneration: a systematic review. *Front. Physiol.* **12**, (2021). 684899.
33. Quinonez-Flores, C. M., Gonzalez-Chavez, S. A. & Pacheco-Tena, C. Hypoxia and its implications in rheumatoid arthritis. *J. Biomed. Sci.* **23**, 62 (2016).
34. Chauhan, S. S. & Warfel, N. A. Targeting PIM kinases to oppose hypoxia-mediated therapeutic resistance. *Oncoscience* **5**, 254–255 (2018).
35. Liu, Y. et al. Pim1 kinase positively regulates myoblast behaviors and skeletal muscle regeneration. *Cell Death Dis.* **10**, 773 (2019).
36. Lim, R., Barker, G. & Lappas, M. Inhibition of PIM1 kinase attenuates inflammation-induced pro-labour mediators in human foetal membranes in vitro. *Mol. Hum. Reprod.* **23**, 428–440 (2017).
37. Liang, C. & Li, Y. Y. Use of regulators and inhibitors of Pim-1, a serine/threonine kinase, for tumour therapy (review). *Mol. Med. Rep.* **9**, 2051–2060 (2014).
38. Gallot, Y. S. & Bohnert, K. R. Confounding roles of ER stress and the unfolded protein response in skeletal muscle atrophy. *Int. J. Mol. Sci.* **22**, https://doi.org/10.3390/ijms22052567 (2021).
39. Afroze, D. & Kumar, A. ER stress in skeletal muscle remodeling and myopathies. *FEBS J.* **286**, 379–398 (2019).
40. Bohnert, K. R., McMillan, J. D. & Kumar, A. Emerging roles of ER stress and unfolded protein response pathways in skeletal muscle health and disease. *J. Cell Physiol.* **233**, 67–78 (2018).
41. Poplawski, T., Pytel, D., Dziadek, J. & Majsterek, I. Interplay between redox signaling, oxidative stress, and unfolded protein response (UPR) in pathogenesis of human diseases. *Oxid. Med. Cell Longev.* **2019**, 6949347 (2019).
42. Li, Y. et al. Changes in serum cytokines may predict therapeutic efficacy of tofacitinib in rheumatoid arthritis. *Mediators Inflamm.* **2019**, 5617431 (2019).
43. Thilagar, S. et al. Comparison of serum tumor necrosis factor-alpha levels in rheumatoid arthritis individuals with and without chronic periodontitis: a biochemical study. *J. Indian Soc. Periodontol.* **22**, 116–121 (2018).
44. Reid, M. B. & Li, Y. -P. Tumor necrosis factor-α and muscle wasting: a cellular perspective. *Respir. Res.* **2**, 269–272 (2001).
45. Li, Y. P. & Reid, M. B. Effect of tumor necrosis factor-alpha on skeletal muscle metabolism. *Curr. Opin. Rheumatol.* **13**, 483–487 (2001).
46. Li, Y. P., Schwartz, R. J., Waddell, I. D., Holloway, B. R. & Reid, M. B. Skeletal muscle myocytes undergo protein loss and reactive oxygen-mediated NF-kappaB activation in response to tumor necrosis factor alpha. *FASEB J.* **12**, 871–880 (1998).
47. Li, X. et al. Cardiac-specific overexpression of tumor necrosis factor-alpha causes oxidative stress and contractile dysfunction in mouse diaphragm. *Circulation* **102**, 1690–1696 (2000).
48. Hardin, B. J. et al. TNF-alpha acts via TNFR1 and muscle-derived oxidants to depress myofibrillar force in murine skeletal muscle. *J. Appl. Physiol.***104**, 694–699 (2008).
49. Langen, R. C. et al. Tumor necrosis factor-alpha inhibits myogenic differentiation through MyoD protein destabilization. *FASEB J.* **18**, 227–237 (2004).
50. Guttridge, D. C., Mayo, M. W., Madrid, L. V., Wang, C. Y. & Baldwin, A. S. Jr. NF-kappaB-induced loss of MyoD messenger RNA: possible role in muscle decay and cachexia. *Science* **289**, 2363–2366 (2000).
51. van Kann, L. N. & Bakker, A. J. Effect of tumor necrosis factor alpha on electrically induced calcium transients elicited in C2C12 skeletal myotubes. *Muscle Nerve* **35**, 251–253 (2007).
52. Frost, R. A., Nystrom, G. J. & Lang, C. H. Lipopolysaccharide regulates proinflammatory cytokine expression in mouse myoblasts and skeletal muscle. *Am. J. Physiol. Regul. Integr. Comp. Physiol.* **283**, R698–R709 (2002).

53. Reid, M. B. & Moylan, J. S. Beyond atrophy: redox mechanisms of muscle dysfunction in chronic inflammatory disease. *J. Physiol.* **589**, 2171–2179 (2011).
54. Larsson, L. et al. Sarcopenia: aging-related loss of muscle mass and function. *Physiol. Rev.* **99**, 427–511 (2019).
55. Rong, Y. D., Bian, A. L., Hu, H. Y., Ma, Y. & Zhou, X. Z. Study on relationship between elderly sarcopenia and inflammatory cytokine IL-6, anti-inflammatory cytokine IL-10. *BMC Geriatr.* **18**, 308 (2018).
56. Consitt, L. A. & Clark, B. C. The vicious cycle of myostatin signaling in sarcopenic obesity: myostatin role in skeletal muscle growth, insulin signaling and implications for clinical trials. *J. Frailty Aging* **7**, 21–27 (2018).
57. Ryan, A. S. & Li, G. Skeletal muscle myostatin gene expression and sarcopenia in overweight and obese middle-aged and older adults. *JCSM Clin. Rep.* **6**, 137–142 (2021).
58. White, T. A. & LeBrasseur, N. K. Myostatin and sarcopenia: opportunities and challenges - a mini-review. *Gerontology* **60**, 289–293 (2014).
59. Kwak, J. Y. & Kwon, K. S. Pharmacological interventions for treatment of sarcopenia: current status of drug development for sarcopenia. *Ann. Geriatr. Med. Res.* **23**, 98–104 (2019).
60. McInnes, I. B. & Schett, G. The pathogenesis of rheumatoid arthritis. *N. Engl. J. Med.* **365**, 2205–2219 (2011).
61. Kruger, K. & Nusslein, H. Cardiovascular comorbidities in rheumatoid arthritis]. *Z. Rheumatol.* **78**, 221–227 (2019).
62. Aletaha, D. et al. 2010 Rheumatoid arthritis classification criteria: an American College of Rheumatology/European League against rheumatism collaborative initiative. *Arthritis Rheum.* **62**, 2569–2581 (2010).
63. Prevoo, M. L. et al. Modified disease activity scores that include twenty-eight-joint counts. Development and validation in a prospective longitudinal study of patients with rheumatoid arthritis. *Arthritis Rheum.* **38**, 44–48 (1995).
64. Martin, M. Cutadapt removes adapter sequences from high-throughput sequencing reads. *EMBnet. J.* **17**, 10–12 (2011).
65. Kersey, P. J. et al. Ensembl Genomes: an integrative resource for genome-scale data from non-vertebrate species. *Nucleic Acids Res.* **40**, D91–D97 (2012).
66. Anders, S., Pyl, P. T. & Huber, W. HTSeq—a Python framework to work with high-throughput sequencing data. *Bioinformatics* **31**, 166–169 (2015).
67. Love, M. I., Huber, W. & Anders, S. Moderated estimation of fold change and dispersion for RNA-seq data with DESeq2. *Genome Biol.* **15**, 550 (2014).
68. Huber, W. et al. Orchestrating high-throughput genomic analysis with Bioconductor. *Nat. Methods* **12**, 115–121 (2015).
69. Mootha, V. K. et al. PGC-1alpha-responsive genes involved in oxidative phosphorylation are coordinately downregulated in human diabetes. *Nat. Genet.* **34**, 267–273 (2003).
70. Subramanian, A. et al. Gene set enrichment analysis: a knowledge-based approach for interpreting genome-wide expression profiles. *Proc. Natl. Acad. Sci. USA* **102**, 15545–15550 (2005).

Acknowledgements

This work was supported by NIH grants UH3TR002142 and R21AR072283. We thank the Duke Genomic Analysis and Bioinformatics Core Facility for RNA-Seq data processing and initial data analysis, including processing and quality control of samples, Principal Components Analysis (PCA) and H-clustering, linear models to compare across treatment and disease types, and gene set enrichment analysis (GSEA) for the results of each comparison was performed by Duke Genomic Analysis and Bioinformatics Core Facility.

Author contributions

G.A.T., W.E.K., K.M.H., and C.E.O.: conception and design of research; C.E.O., J.L.C., and M.X.: performed experiments; C.E.O., J.L.C., M.X., and J.S.H.: analyzed data; C.E.O., M.X., and G.A.T.: interpreted results of experiments; C.E.O. and G.A.T. prepared figures; C.E.O., G.A.T.: drafted manuscript; C.E.O, W.E.K., K.M.H, and G.A.T.: edited and revised manuscript; C.E.O. and G.A.T.: reviewed and approved final version of manuscript.

Competing interests

The authors declare no competing interests.

Ethics approval

This study complied with the Helsinki Declaration and was approved by the Duke University Institutional Review Board.

Additional information

Supplementary information The online version contains supplementary material available at https://doi.org/10.1038/s42003-025-07970-8.

Correspondence and requests for materials should be addressed to George A. Truskey.

Peer review information *Communications Biology* thanks Chowdhury Abdullah, Songtao Fan, and Veronica Azcutia for their contribution to the peer review of this work. Primary Handling Editor: Manuel Breuer. A peer review file is available.

Reprints and permissions information is available at http://www.nature.com/reprints

Publisher's note Springer Nature remains neutral with regard to jurisdictional claims in published maps and institutional affiliations.

Open Access This article is licensed under a Creative Commons Attribution-NonCommercial-NoDerivatives 4.0 International License, which permits any non-commercial use, sharing, distribution and reproduction in any medium or format, as long as you give appropriate credit to the original author(s) and the source, provide a link to the Creative Commons licence, and indicate if you modified the licensed material. You do not have permission under this licence to share adapted material derived from this article or parts of it. The images or other third party material in this article are included in the article's Creative Commons licence, unless indicated otherwise in a credit line to the material. If material is not included in the article's Creative Commons licence and your intended use is not permitted by statutory regulation or exceeds the permitted use, you will need to obtain permission directly from the copyright holder. To view a copy of this licence, visit http://creativecommons.org/licenses/by-nc-nd/4.0/.

© The Author(s) 2025, corrected publication 2025